Light Metals 2013 *Edited by: Barry Sadler*
TMS (The Minerals, Metals & Materials Society), 2013

Frequency response analysis of anode current signals as a diagnostic aid for detecting approaching anode effects in aluminum smelting cells

C. Cheung, C. Menictas, J. Bao, M. Skyllas-Kazacos, B. J. Welch
School of Chemical Engineering, the University of New South Wales, Sydney NSW 2052, Australia

Keywords: Individual anode current, Anode effect, Early fault detection

Abstract

Modern cell control aims to prevent anode effects by controlling the alumina feeding rate based on the change in cell resistance or voltage and the preset limits of these values. Success of this approach depends on the uniform distribution of dissolved alumina across the cell and the anode current distribution. As this is not always the case in practice, the control procedure sometimes fails and the cell undergoes anode effect. Monitoring of the anode current signals has been suggested as an alternative way for early anode effect detection. This paper presents frequency response analysis of anode current signals obtained from an operating cell and shows the ability for early detection of an anode effect. It has been found that the frequency response peak associated with bubble dynamics of the corresponding anode disappears as it undergoes partial anode effect prior to the cell approaching full anode effect. The results show that the analysis can provide further information to identify a localized anode effect which can facilitate cell control for more effective anode effect prevention.

Introduction

An anode effect is a process abnormality in the Hall Héroult process. It arises when anodes are passivated by an insulating layer of bubbles produced by carbon side reactions when the alumina concentration at the anode surface is depleted, leading to concentration polarization and the discharge of fluoride ions [1]. This causes an increase in electrical resistance at the anode-bath interface as the non-conductive layer blocks the passage of current. An anode effect often starts at a localized level due to local depletion of alumina before it propagates across the cell [2, 3]. Its occurrence is undesirable as it disrupts normal reaction, leading to reduction of current efficiency, increase of energy consumption as well as PFC emissions [4]. An onset of an anode effect is normally detected from a sudden increase in cell voltage [5]. This method, however, only provides a warning when the cell goes into anode effect, leaving little time for remedial actions to be carried out. In noisy cells, voltage noise can sometimes mask the cell voltage increase [6]. Early anode effect detection based on the cell voltage signal may fail as the cell voltage only reflects the overall cell condition. As a result, cell voltage signals may not be sufficient for achieving effective detection in order to eliminate or inhibit the onset of an anode effect.

Application of anode current signals

Several anode effect predictors based on cell voltage measurements have been developed to improve detection of an impending anode effect [7-10]. However, they are still unable to pinpoint the rise of a local or partial anode effect. Individual anode current measurements, on the other hand, can compensate this deficiency as they provide spatial information on the cell [11]. The magnitude of the current flowing into each anode is determined by the combined electrical resistances in the respective current path. The path resistance is governed by anodic process dynamics and the bath conditions in the vicinity of the anode. As the line current is regulated in the process, anode currents redistribute when a variation in the path resistance arises. As a result, monitoring individual anode current signals allows supervision of local cell conditions, and thus fault detection at a localized level.

Various studies have investigated individual anode currents of industrial reduction cells in the lead up to an anode effect [11-14]. They show that anode currents redistribute before the sudden rise of cell voltage. It has been suggested that a reduction in anode current observed at some anodes during current redistribution is an indication of the beginning of local anode effect at the respective anodes. These studies demonstrate the potential application of monitoring the individual anode current signals in order to achieve early detection and isolation of an impending anode effect. Although the interval between anode current redistribution and cell voltage increase varies in different studies, it provides additional time for control actions to take place before, rather than at the onset of the anode effect. These studies, however, only analyze the change of signal response in the time domain. This may not be sufficient for an accurate detection of an impending anode effect as other abnormal events such as a slipped anode, can cause a decrease in anode current of a nearby anode upon anode current redistribution.

This paper presents the characterization of anode current signal responses measured from an industrial reduction cell in both time and frequency domain. Signal responses during normal operating conditions are first studied and compared with those obtained in abnormal conditions. The study demonstrates that local anode effects can be detected and isolated more precisely when the detection is based on time domain together with frequency response analysis. Besides anode effect, deliberate disturbances were introduced to the cell to induce anode current reduction on some anodes, similar to what occurs before the onset of an anode effect. Frequency responses of the signals obtained in both abnormalities are compared. Differences observed in the frequency domain representation are also discussed. This work shows frequency analysis of anode current signals provides supplementary information about the cell condition. The combination of time domain and frequency domain processing of anode current signals allows more effective and earlier identification of an impending anode effect. Further studies can lead to the development of an early anode effect detection and isolation system.

Anode effect

The selective evolution of carbon oxides during normal electrolysis of cryolite alumina melts is dependent on the anode polarization remaining below approximately 0.7V referenced against pure carbon dioxide evolution in an alumina saturated solution. An increase in the anode potential above that\ limit leads to the coevolution of COF_2. Its formation results in generations of CO and CF_4 ($\Delta G° = -45.77$ kJ at 960°C) according to the reaction [15]:

$$2COF_2 + C = 2CO_{(g)} + CF_{4(g)} \quad (1)$$

Various operation conditions can cause the increase of the anode potential, including: Increase in current density or aluminum fluoride concentration, decreased stirring or agitation, and depletion of the alumina concentration [16]. Once fluoride ion co-deposition is initiated on a carbon surface enabling the above reaction, a resistive intermediate surface layer forms, probably due to the kinetics of the product desorption reactions. It can lead to partial or total passivation of the anode surface, depending on the voltage and other cell conditions [17, 18]. Under galvanostatic conditions, the formation leads to an increase in cell voltage with arcing occurring at the electrode as the product gases are evolved. The dominant products are CO and CF_4 [19]. The latter is the characteristics of the abnormal condition normally referred as to an anode effect.

The changed interfacial conditions due to the co-deposition of fluoride ions results in a change in the interfacial tensions and wetting angle. The combination of these events causes the formation of larger bubbles on the horizontally oriented surface of an anode underside. This further inhibits the current flow in that zone [20]. The generation of the gases therefore shifts to the vertically oriented sides of the anode where gas release is easier; especially with the aid of the higher temperatures generated by the arcing.

In an operating cell, the situation is more complex. There are not only spatial variations in alumina concentration, but also total voltage control for each anode (as opposed to anode potential control), while the cell as a whole is under current control. Thus, as an anode initiates the co-deposition of fluoride and forms various products, the current is expected to reduce. That means more current flows to other anodes, leading to uneven current distribution. The increase in anode current in those anodes accelerates the depletion rate of local alumina concentration, thus driving local conditions further to the extreme condition. The formation of larger bubbles under the anode that initially start the fluoride co-evolution combined with the shift in current to the sides of the anode might be expected to change the frequency of the bubble release as well as its intensity.

Bubbling process

Studies show that bubbles release contributes to the prominent peak in the frequency response of the signals at around 1 Hz, under normal conditions [21]. The actual range can vary depending on the cell technology and anode configuration. As the amplitude of the peak on the spectrum reflects the intensity of the bubbles escaping from an anode, the variation of the peak indicates the change of bubble properties caused by varying local conditions. Therefore, we have explored whether frequency analysis of anode current signals can be used to detect an impending anode effect by comparing the reduction of bubble release with the release behavior during normal operation.

Measurements setup

There are a number of considerations that need to be taken into account when setting up a data acquisition system for collecting individual anode current signals. Of primary importance is the method used to measure individual anode current signal on the anode rod and the method used to transmit the signals to the recording device or control system.

Anode current signals measurement devices

In this study, the individual anode current signals on the anode rods were determined by measuring the voltage drop over a set distance between the bottom of the anode beam and above the cell hood. The available distance on the anode rods in this location was less than 3cm which resulted in an expected voltage drop over this distance in the order of 10^{-4} volts. Therefore, signal amplification at the signal source was required with a gain of 100 in order to have an adequate signal to noise ratio in the signals reaching the data acquisition system.

Specific individual signal amplifiers were designed and fabricated. These amplifiers were mounted near the signal source on the anode beam and were powered by a DC voltage with the required input voltage in the range of 5-15V. The componentry of the signal amplifiers required a low temperature drift in the gain and in order to maintain stable amplification at elevated temperatures. An additional limitation was that the temperature in this area of the beam could reach temperatures above 70°C, therefore, two AA type lithium thionyl chloride high temperature batteries with an operating range of over 85°C were connected in series providing 7.2 V power input to each signal amplifier.

The signal wiring employed to carry the anode current signal from the signal source on the individual anode rods to the data acquisition system was two core high temperature wire. It provided differential voltage input signals to the data acquisition system. In order to correctly estimate the individual anode current from the measure anode rod voltage drop readings, the resistance of the anode rod material in the location of the voltage drop measurement is required. As resistance of the anode rod varies with temperature, the temperature at each voltage drop measurement was measured using type K Teflon coated thermocouple wire. All wiring was secured in high temperature wiring looms and held securely in place to limit possible damage during cell operation.

Data acquisition system and software interface

The data acquisition system used to collect the individual anode rod voltage drop measurements was a National Instruments NI Compact Rio. This real-time controller employs an on-board 800 MHz controller and 4GB of solid state memory. The controller was also fitted to a four slot chassis which in turn was fitted with two analog (voltage) input modules and two thermocouple input modules. The data acquisition system was powered by DC battery packs. The system was found to operate successfully in the harsh temperatures and high magnetic fields existing in the aluminum reduction cell operating environment. The data

acquisition system was programmed using Labview. The data were collected with the sampling rates between 30 Hz and 10 Hz.

The user interface constructed in Labview, as shown in Figure 1, consists of a graphical representation of the individual anode currents (represented as mV drop readings). In addition, the temperature at each corresponding measurement location is shown together with other parameters such as time, date, data scan rates and data file paths.

In addition to providing the options for data sampling and handling, the above graphical user interface presents the operator in real-time the anode current distribution within the cell.

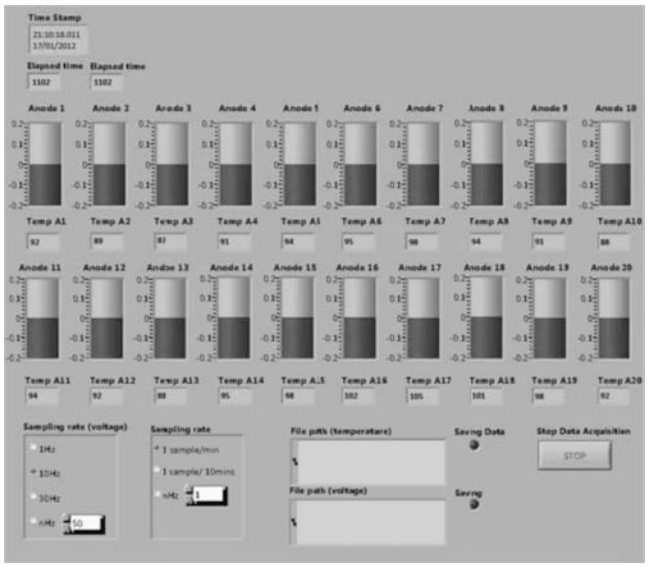

Figure 1 Interface of the data acquisition system

Data analysis

In this work, anode current signals were measured at a sampling rate of 10 Hz in an operating reduction cell equipped with point feeders. The sampling rate was chosen as it covered the frequency range corresponding to bubbles releases as reported in the literature [21]. The study examines the frequency response of current signals obtained during normal operation and compares it with those responses under abnormal conditions. Frequency responses of the anode signals were generated by fast Fourier transform (FFT) with a window size of 1 minute (i.e. 600 data points). Analyses of signals responses in all cases are presented and discussed in the following sections.

Results and Discussions

Normal operating response

The typical frequency response of anode current signals during normal operation is shown in Figure 2. The signals were acquired from an anode without any slot features. The prominent peak observed in the frequency range of 0.8-1.2 Hz is contributed by the bubbles releases, similar to responses found in the literature [22]. This peak is found in all frequency response analyses of anodes with the same configuration, although it may show slight variations in amplitude and frequency. Several factors such as anode current density and anode shape can lead to such differences in the peak [23]. The correlation between the peak properties and cell conditions is not further investigated in this paper as it is not the primary focus of the study.

Minor peaks sometimes also appear in the power spectrum, as illustrated in Figure 2. In the case shown in the figure, these peaks occur at the frequency of 1.6 z and 2.5 Hz and suggest that there were some bubbles released at a faster rate. These peaks only appear intermittently in the spectrum and do not sustain like the prominent peak when the frequency response changes with the moving window.

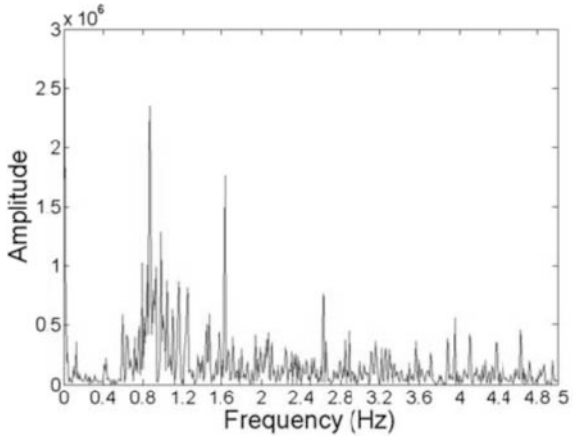

Figure 2 Typical Frequency response of typical anode current signal during normal operation.

Abnormal operating response

Anode slippage and anode effect are the abnormalities studied in the present work. They both lead to anode current redistribution. However, their impacts on bubble dynamics are different. These abnormalities were introduced to the cell at different time, so that their impact could be investigated separately. Slippage of an anode was simulated by lowering an anode by 2 cm. The onset of an anode effect was introduced by manually blocking a feeder to reduce alumina concentration. The cell layout is shown in Figure 3 marked with anode numbers. The location of the lowered anodes and the blocked feeder are also highlighted in the figure.

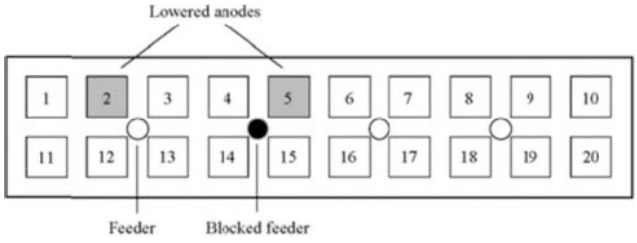

Figure 3 Anode numbering layout and feeders locations in the reduction cell

Anode slippage

Anode slippage describes a condition when an anode slides down into the bath unintentionally because it is not held by the clamp properly. Its occurrences gives rise to anode current redistribution as the slipped anode draws more current due to its relatively small path resistance. Its impact on the current distribution was simulated by lowering an anode. The resulting current profiles of lowered anodes and a nearby anode are shown in Figure 4. Current drawn by Anodes 2 and 5 increased as they were lowered during the experiment. Current redistributed and led to a reduction of current on Anode 1.

Frequency response of anode current signals measured from Anode 2 is presented in Figure 5. The power spectrum before the anode was lowered shows the prominent peak as expected in normal operating condition with little noise at the high frequency range. The response became nosier after the anode was lowered. This was because more bubbles were formed when the anode carried higher current as predicted by the Faraday's law. The intensified bubble formation not only increases the bubble induced resistance, but also restricts the time of the bubbles retained underneath the anode. Bubbles therefore escaped faster than before the anode being lowered. This led to the bubbles release rate broadened to the higher end of the frequency range as reflected on the spectrum. The amplitude of the response is also amplified. A similar response is observed from the spectrum of Anode 5.

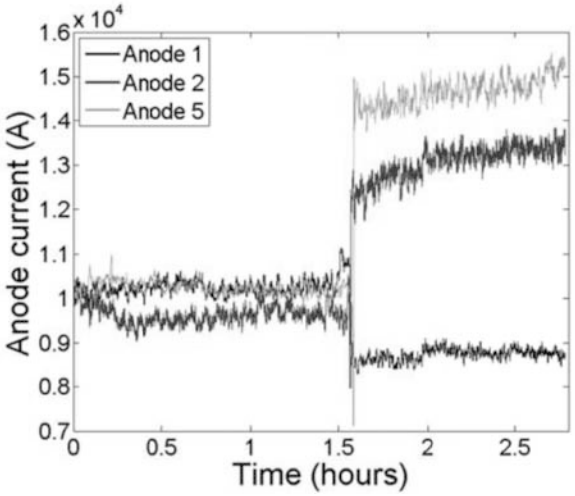

Figure 4 Current profiles of two lowered anode (Anode 2 and 5) and a nearby anode (Anode 1).

As suggested by Faraday's law, an anode that carried less current would produce less carbon dioxide gas bubbles. The reduction of bubble release is observed from the response of Anode 1 as shown in Figure 6. The amplitude of the signal reduces as bubble induced resistance becomes smaller.

Anode effect

The current profiles of anodes near the blocked feeder and the change of voltage as the cell entered anode effect are shown in Figure 7. A slight increase in voltage (4.75 V) occurred less than one minute before the onset of the anode effect as reflected by the high voltage measured from the cell (21.77 V). Anode currents, on the other hand, showed a sign of current reduction at Anode 15 almost two and a half minute before the sudden increase of voltage, as marked by an arrow. Similar anode current distribution before the onset of an anode effect is also reported in the literature [24], suggesting an early sign of an approaching anode effect. Anode current redistribution illustrates how the anode effect starts at a localized level before propagating to the entire cell. The reduced current flow is caused by the increase bubble induced resistance as perfluorocarbon gases start to passivate the anode surface. Although anode current reduction can be an indicator of a cell leading to anode effect, it can also be caused by other factors such as anode cathode distance reduction of other anodes as demonstrated by anode slippage experiment.

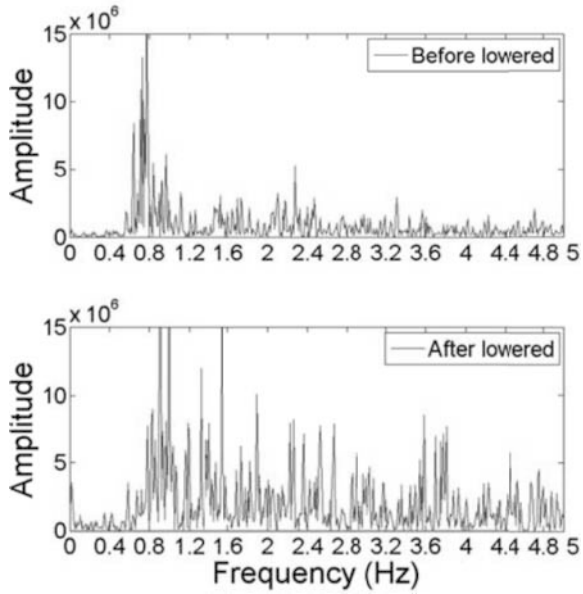

Figure 5 Frequency responses of Anode 2 before (above) and after (below) it is lowered.

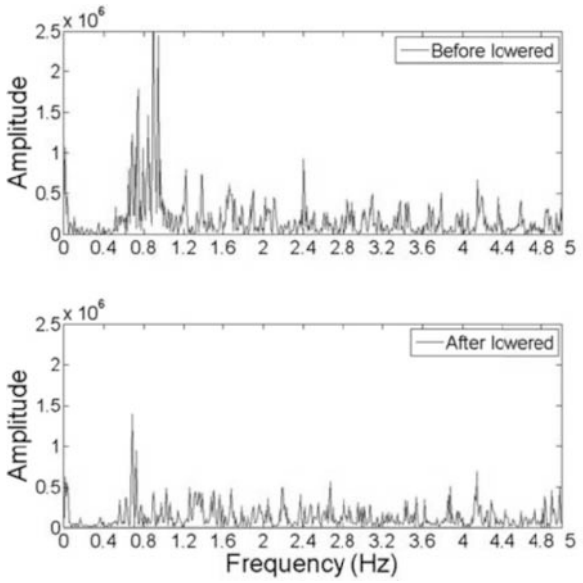

Figure 6 Frequency responses of Anode 1 before (above) and after (below) Anode 2 is lowered.

As a result, an alternative method is required to discriminate anode effect from other abnormalities. Figures 8 – 10 show frequency responses of two anodes (Anodes 14 and 15) at different stages, annotated in Figure 7. Frequency response of Anode 14 is chosen to compare with Anode 15 as it does not show any significant change until the onset of the anode effect. At Stage A, both spectra show prominent peaks formed in the range of 0.8 – 1 Hz, as depicted in Figure 2 during normal operation. As anode current of Anode 15 reduced in Stage B, the peak reduced significantly whereas the peak on the spectrum of anode 14 occurred at a similar frequency and amplitude as in Stage A. Both responses carried on to Stage C before the cell entered anode effect. The differences in signal response of Anodes 14 and 15 proved anode effect started at a localized level before spreading out across the cell.

Beside the significant reduction of the peak, the spectrum of Anode 15 became less noisy. The rate of noise reduction was greater, when compared to the spectrum of the Anode 1, which carried less current shown in Figure 6. The greater reduction in peak and noise was caused by two mechanisms: Reduction of carbon dioxide gas generation and formation of perfluorocarbon gases. Fewer carbon dioxide gas bubbles were generated at the anode as anode current decreased. Its effect on the frequency response was discussed in the previous section. On the other hand, as local anode effect started at the anode, perfluorocarbon gases began to form. The formation of perfluorocarbon gases caused fewer bubbles to release from the anode as the bubbles tended to adhere on the surface. The combination of these two mechanisms gives rise to a different response from the case where current reduced merely due to the change of relative anode cathode distance. The frequency response of anode current signals thus can help to distinguish an approaching anode effect from other abnormalities that cause a reduction in anode currents.

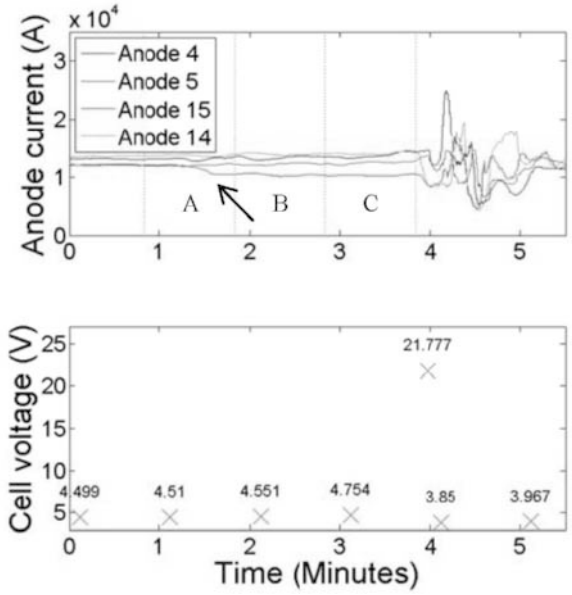

Figure 7 Current profiles of the anodes around the blocked feeder (above) and the respective cell voltage (below).

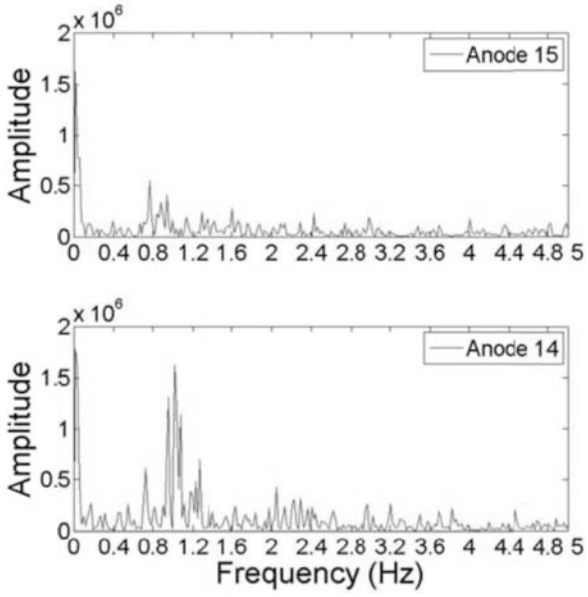

Figure 8 Frequency responses of Anode 15 (above) and 15 (below) in Stage A of anode effect (Figure 7).

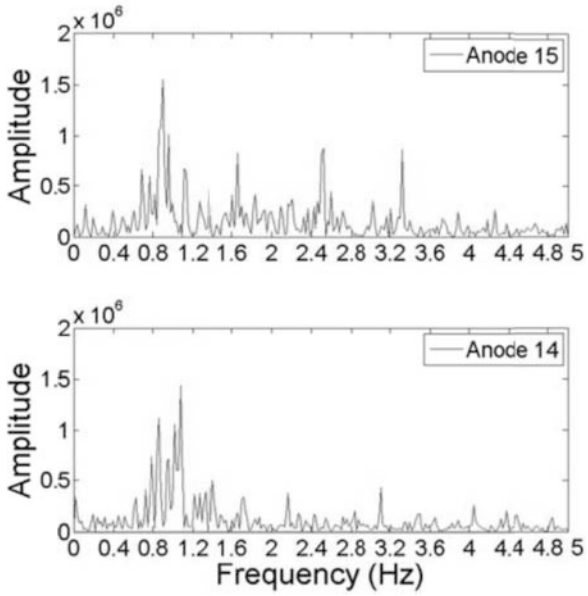

Figure 9 Frequency responses of Anode F3 (above) and F4 (below) in Stage B of anode effect (Figure 7).

Conclusion

The present work shows frequency analysis of anode current signals achieves better prediction of an approaching anode effect compared with time domain analysis. Different from other studies in the literature, signal responses of anode current in the frequency domain are investigated in this work. It is shown that bubble dynamics is closely related to the local condition within the cell, and is reflected by the frequency response of the individual anode current signals. The combination of frequency domain and time domain analysis can therefore improve the precision of detecting an approaching anode effect by

discriminating it from other cases that have similar effect on the signals in time domain.

Acknowledgement

This project is financially supported by the CSIRO Cluster on Breakthrough Technologies for Aluminium Production, in collaboration with Dubai Aluminium Company Ltd. In particular, authors acknowledge the kind support and assistance on the experiments from Dr. Maryam Mohamed Al-Jallaf, Dr. Daniel Whitfield, Dr. Adam Sherrif and Mr. Ali Jassim.

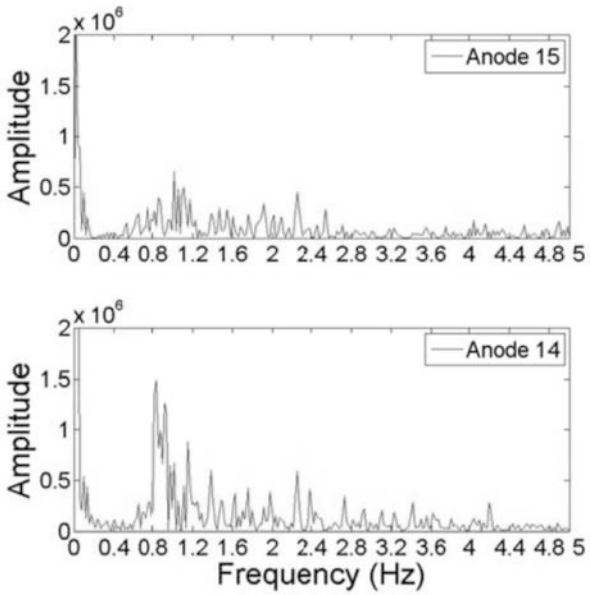

Figure 10 Frequency responses of Anode F3 (above) and F4 (below) in Stage C of anode effect (Figure 7).

Reference

1. Thonstad, J., et al., *Aluminium electrolysis : fundamentals of the Hall-Héroult process* (Düsseldorf : Aluminium-Verlag, 2003) .
2. Thonstad, J. and H. Vogt. *Terminating anode effects by lowering and raising the anodes - A closer look at the mechanism*. in *Proceedings of TMS Light Metals*. 2010. Seattle, WA, 461-466 .
3. Thonstad, J., et al. *On the anode effect in industrial aluminium cells*. in *Proceedings of TMS Light Metals*. 1984. Warrendale, PA, 249-256.
4. Grjotheim, K. and B.J. Welch, *Aluminium smelter technology - A pure and applied approach* (Aluminium-verlag Gmbh Dusseldorf) 1980.
5. Bearne, G., *The development of aluminum reduction cell process control*. JOM Journal of the Minerals, Metals and Materials Society, 51 (1999), 16-22.
6. Haupin, W. and E.J. Seger. *Aiming for zero anode effects*. in *Proceedings of TMS Light Metals*. 2001. New Orleans, LA, 329-335.
7. Sulmont, B., et al. *The new development of the ALPSYS system related to the management of anode effect impact*. in *Proceedings of TMS Light Metals*. 2006. San Antonio, TX, 325-329.
8. Delclos, C. and O. Bonnardel, *Method and device for detecting anode effects of an electrolytic cell for aluminum production*, 2007, US 7175749 B2.
9. Bell, D.G., *System for predicting impending anode effects in aluminum cells*, 2000, US 6132571.
10. Costa, F.d., et al., *Computer algorithm to predict anode effect events*, in *Proceeding of TMS Light Metals*2012: Orlando, FL. p. 655 - 656.
11. Keniry, J.T., et al. *Digital processing of anode current signals: An opportunity for improved cell diagnois and control*. in *Proceedings of TMS Light Metals*. 2001. New Orleans, LA, 1225 - 1232.
12. Keniry, J. and E. Shaidulin, *Anode signal analysis - The next generation in reduction cell control*, in *Proceedings of TMS Light Metals* 2008 , New Orleans, LA 287-292.
13. Steingart, D., et al. *Experiments on wireless measurement of anode current in Hall cells*. in *Proceedings of TMS Light Metals*. 2008. New Orleans, LA, 333-338.
14. Evans, J.W. and N. Urata. *Technical and operational benefits of individual anode current monitor*. in *Proceedings of 10th Australian Aluminium Smelting Technology Conference*. 2011. Launceston, TAS.
15. Dorreen, M.M.R., et al. *Sulfur and fluorine containing anode gases produced during normal electrolysis and approaching an anode effect*. in *Proceedings of TMS Light Metals*. 1998. San Antonio, TX, 311-316.
16. Richards, N.E. and B.J. Welch. *Anodic Overpotentials and Mechanisms of the Anode Process on Carbon in Cryolite-Alumina Electrolytes*. in *Proceedings of the first Australian Conference on Electrochemistry*. 1964. Sydney, 901-922.
17. Haverkamp, R.G., *Surface studies and dissolution studies of fluorinated alumina*, 1992, Ph.D thesis, University of Auckland.
18. Frazer, E.J. and B.J. Welch. *Reactions occurring at the anode during aluminium electrowinning*. in *Proceedings of Aus. I. M. & M.* 1976, 17-22.
19. Tabereaux, A.T., N.E. Richards, and C.E. Satchel. *Composition of Reduction Cell Anode Gas during Normal Conditions and Anode Effects*. in in *Proceedings of TMS Light Metals*. 1995. Las Vegas, NV, 325-333.
20. Meunier, P., *Electrochemical study of the anode effect in aluminium reduction cells*, 2004, Ph.D thesis, University of New South Wales.
21. Wang, X. and A.T. Tabereaux. *Anodic phenomena - observations of anode overvoltage and gas bubbling during aluminum electrolysis*. in *Proceedings of TMS Light Metals*. 2000. San Diego, CA, 1-9.
22. Kiss, L.I. and S. Poncsák. *Effect of the bubble growth mechanism on the spectrum of voltage fluctuations in the reduction cell*. in *Proceedings of TMS Light Metals*. 2002. Seattle, WA, 217-223,
23. Poncsák, S., et al. *Size distribution of the bubbles in the Hall-Héroult cells*. in *Proceedings of TMS Light Metals*. 2006. San Antonio, TX, 457-461.
24. Evans, J.W. and N. Urata, *Technical and operational benefits of individual anode current monitor*, in *Proceedings of 10th Australian Aluminium Smelting Technology Conference* 2011. Launceston, TAS.